Modulating Magnetism in Ferroelectric Polymer-Gated Perovskite Manganite Films with Moderate Gate Pulse Chains

Hon Fai Wong[1], Sheung Mei Ng[1], Wen Zhang[2,3], Yu Kuai Liu[1], Ping Kwan Johnny Wong[2,4], Chi Sin Tang[3], Ka Kin Lam[1], Xu Wen Zhao[1], Zhen Gong Meng[5], Lin Feng Fei[1], Wang Fai Cheng[1], Danny von Nordheim[6], Wai Yeung Wong[7], Zong Rong Wang[8], Bernd Ploss[6], Ji-Yan Dai[1], Chee Leung Mak[1], Andrew Thye Shen Wee[3,4], Chi Wah Leung[1]*

[1] Department of Applied Physics, The Hong Kong Polytechnic University, Hung Hom, Kowloon, Hong Kong, China

[2] School of Electronics and Information and School of Microelectronics, Northwestern Polytechnical University, 127 West Youyi Road, Xi'an, Shaanxi, 710072, China

[3] Department of Physics, National University of Singapore, 2 Science Drive 3, Singapore 117542, Singapore

[4] Centre for Advanced 2D Materials and Graphene Research Centre, National University of Singapore, 6 Science Drive 2, Singapore 117546, Singapore

[5] College of Chemistry and Environmental Engineering, Shenzhen University, Shenzhen 518060, China

[6] Department of SciTec, University of Applied Sciences Jena, Carl-Zeiss-Promenade 2, 07743 Jena, Germany

[7] Department of Applied Biology and Chemical Technology, The Hong Kong Polytechnic University, Hung Hom, Hong Kong, China

[8] State Key Lab of Silicon Materials, School of Materials Science and Engineering, Zhejiang University, Hangzhou, China

* dennis.leung@polyu.edu.hk

ABSTRACT

Most previous attempts on achieving electric-field manipulation of ferromagnetism in complex oxides, such as $La_{0.66}Sr_{0.33}MnO_3$ (LSMO), are based on electrostatically-induced charge carrier changes through high–k dielectrics or ferroelectrics. Here the use of ferroelectric copolymer, polyvinylidene fluoride with trifluoroethylene [P(VDF-TrFE)], as a gate electrode to successfully modulate the ferromagnetism of LSMO thin film in a field-effect device geometry is demonstrated. Specifically, through the application of low voltage pulse chains inadequate to switch the electric dipoles of the copolymer, enhanced tunability of the oxide magnetic response is obtained, compared to that induced by ferroelectric polarization. Such observations have been attributed to electric-field-induced oxygen vacancy accumulation/depletion in the LSMO layer upon the application of pulse chains, which is supported by element-specific characterization techniques, including X-ray photoelectron spectroscopy and X-ray magnetic circular dichroism. These techniques not only unveil the electrochemical nature of the mechanism but also establish a direct correlation between the oxygen vacancies created and subsequent changes to the valence states of Mn ions in LSMO. These demonstrations based on the pulsing strategy can be a viable route equally applicable to other functional oxides for the construction of electric-field-controlled magnetic devices.

1. INTRODUCTION

Doping is frequently adopted for manipulating the transport and magnetic properties of complex oxides. [1-4] Recent efforts include, for instances, electrostatic gating of charge carriers at oxide interfaces, across high–k dielectrics [5, 6] or ferroelectrics. [5-7] Such electric-field-induced modulation schemes permitted a change in the areal charge density below $10^{14} \, cm^{-2}$. Electrolytes or ionic liquids (IL) can achieve stronger modulation via the electric-double-layer (EDL) effect, [8, 9] capable of an interfacial capacitance up to tens of $\mu F\text{-}cm^{-2}$ (a change of $\sim 10^{15} \, cm^{-2}$ in carrier density). [9] Such modulation has been shown to remain effective even with the gate voltage retracted, [10] which arises due to the redox reactions between IL and the channel layer. [11-15] Yet, this may necessitate a protective layer in some cases. [16] The strong modulation effect by IL has facilitated the observation of various exotic phenomena, such as tunable metal-insulator transition in manganites, [13, 17] and modulation of superconductivity in two-dimensional layered materials. [18, 19]

Previous attempts on electric-field-induced magnetism modulation in perovskite manganites rely on epitaxially-grown oxide ferroelectrics. [7, 20-23] Charge carriers at the ferroelectric/manganite interfaces were manipulated through polarization switching, thus achieving changes in the transport and magnetic behavior. This scheme, however, poses practical challenges for probing the interfacial changes at the manganite layer upon ferroelectric reversal. Polyvinylidene fluoride with trifluoroethylene [P(VDF-TrFE)], a typical ferroelectric copolymer, can be a promising alternative in this regard due to its solubility in organic solvents. [24] This therefore enables direct access to the interfacial changes in the magnetic perovskite by conventional surface-sensitive techniques. Besides, the copolymer exhibits other favorable features for realizing electric-field

controlled devices, including low processing temperature (~140°C), [25-27] chemical inertness and high compatibility with various types of magnetic materials. [28]

Here, we report a pilot study on the use of P(VDF-TrFE) as a top gate dielectric for non-volatile, electrical control of transport and magnetic properties in epitaxial $La_{0.66}Sr_{0.33}MnO_3$ (LSMO)-based field-effect-transistor (FET). Instead of using a large saturation voltage that can lead to dielectric breakdown, [20, 21] we demonstrate a low-voltage pulsing scheme by an applied voltage lower than the threshold for ferroelectric switching and realize gradually modulated magnetism in the LSMO active layer. Combining X-ray photoemission spectroscopy (XPS) and X-ray magnetic circular dichroism (XMCD), we further establish the correlation between the electrochemical nature of the pulsing process and the manganite surface magnetic moments, in which oxygen vacancies created in the LSMO at its interface with the copolymer play a very crucial role.

2. EXPERIMENTAL SECTION

2.1 Thin Film Growth

LSMO films (7.5 nm) were grown on STO (001) single-crystal substrates, by means of pulsed laser deposition from a stoichiometric target at substrate temperature of 700°C and an oxygen ambient of 150 mTorr. [29-31] While ultrathin layers allow more prominent tunability, dead-layer (2 – 4 nm) are known to form in ultrathin films and would not show magnetism. [32] The current LSMO thickness is a compromise for preserving the magnetic properties while allowing sizable tuning effects. The samples were post-annealed for 5 minutes *in situ* with 10 Torr of oxygen, before they were cooled to room temperature at 10 K/min.

2.2 Device Fabrication

To prepare the FET-type devices, the LSMO layer was patterned into Hall bars (channel length 200 μm, channel width 20 μm) by photolithography and inductively coupled plasma etching. Ti (15 nm)/Au (80 nm) electrodes were deposited by electron beam evaporation under a base pressure of 5×10^{-4} Pa. For the ferroelectric copolymer gates (~ 250 nm), P(VDF-TrFE) with 7:3 molar ratio of VDF and TrFE copolymers was dissolved in diethyl carbonate. The solution was spin-coated and subsequently annealed at 120ºC for two hours to achieve ferroelectric β phase. [25, 26] Al(100 nm)/Au(30 nm) top gate electrodes were prepared by electron beam evaporation through a stainless steel shadow mask.

2.3 Structural Characterization

X-ray diffraction (XRD) and X-ray reflectivity (XRR) measurements were conducted using a high-resolution X-ray diffractometer with Cu-K_α radiation (Rigaku, SmartLab). The thickness of LSMO is determined using a pre-calibrated growth rate through the XRR measurement. X-ray photoelectron spectroscopy (XPS) was performed with a Sengyang SKL-12 electron spectrometer equipped with a VG CLAM 4 MCD electron energy analyzer and twin anode Mg K_α or Al K_α radiation X-ray sources. The base pressure for the XPS measurement was 2×10^{-9} Torr. All binding energies in this work were calibrated to the C *1s* peak (284.6 eV). Cross-sectional transmission electron microscopy (TEM) imaging was performed (JEOL, JEM-2100F).

2.4 X-ray Absorption (XA) and Magnetic Circular Dichroism (XMCD) Measurements

XA/XMCD spectra were collected at Mn $L_{2,3}$ edge in total-electron-yield mode using circularly polarized X-rays. The angle of incidence of the photon beam was set to 60° (grazing incidence) with respect to the sample surface normal. After normalization to the incident beam intensity, the XMCD was obtained as the difference between the two XAS measured with opposite

magnetization directions. Measurements were carried out at ~77 K at the Surface, Interface and Nanostructure Science (SINS) beamline at the Singapore Synchrotron Light Source. [33]

3. RESULTS AND DISCUSSION

3.1 Microstructural and Transport Behavior

Microstructural characterization and ferroelectric measurements have established the high quality of LSMO films and ferroelectric nature of the copolymer films used for this work (**Figure S1**, Supporting Information). The deposition of copolymer on LSMO layer did not induce structural distortion (TEM image in Figure S1) and change of magnetic properties (preserve of Tc regardless of treatments). To investigate resistance modulation, LSMO films were patterned into the top-gate FET geometry (**Figure 1**(a)). [34] Depending on the magnitude of gate voltage (V_g), pulse width and pulse number (**Figure S2**), a gradually modulated channel resistance (R_{xx}) was achieved by using chains of moderate V_g pulses insufficient to switch the gate ferroelectric polarization. This scheme opens up a potential pathway for robust multilevel memory applications, [29, 35] which is otherwise unlikely for devices operating with a large saturation gate voltage that could lead to dielectric breakdown.

Temperature-dependent resistance (R–T) measurement was used to monitor the variation of magnetism in LSMO. The trace peak in such measurement corresponds to the Curie temperature (T_C) of the oxide, due to its origin from the metal-insulator transition. [4] As such, Figure 1(b) shows the temperature-dependent R_{xx} of LSMO channel after applying $+V_g$ pulses at 300 K; unless otherwise stated the magnitude of V_g is kept at 10 V for all measurements shown later in this paper. It is apparent that R_{xx} shows an increasing trend, with its peak shifting gradually towards lower temperatures for rising number of $+V_g$ pulse counts. The variation in T_C has been

derived from Figure 1(b) and plotted against the pulse counts (Figure 1(c)), indicating a reduced T_C of LSMO channel from 280 K (before pulses applied) to 265 K (after 36k pulses). Considering the concomitant increase in R_{xx} of the channel (inset of Figure 1(c)), we propose hole depletion from the LSMO channel upon the application of $+V_g$ pulses as the source of reduced T_C, which can be described by $\frac{\Delta\rho}{\rho} \propto \frac{\Delta T_C}{T_C}$, where ρ is the hole concentration in LSMO. [6] Following this correlation, a shift of T_C by 15 K as in our experiment corresponds to a 7 % variation of ρ (more discussion on the mechanism in latter sections).

Figure 2(a) shows the magnetoresistance (MR) of the LSMO channel at 20 K as a function of $+V_g$ pulse counts, where MR is defined as $(R_{xx}(B) - R_{xx}(B=0))/R_{xx}(B=0))$ and B is the external magnetic field. The channel is seen to exhibit increasingly negative MR. For example, at $B = 0.12$ T, the MR without V_g is –0.65 %, and increases to –1.15 % with 36k $+V_g$ pulses (Figure 2(b)). We note that this observation shows good agreement with the magnetic degradation in the LSMO as proposed above, which could lead to increase in spin-disorder sites and magnetic inhomogeneities in the oxide channel. [36] Smaller magnetic field were required to align these spin-ordered sites in the weakly localized regime upon the increase in V_g pulsing. Therefore, the more negative MR is expected as in Figure 2(a).

3.2 Reversible Switching of R_{xx}

The direction of resistance change is closely linked to the sign of V_g pulses. **Figure 3** shows the LSMO channel resistance corresponding to the sign change of V_g from positive (*i.e.* gate electrode at higher potential than drain electrode) to negative after 36k pulses. With $+V_g$, ΔR_{xx} shows a continuous increase up to 45% of channel resistance before pulses (defined as R_o), which gradually returns to its initial value when the sign of V_g is reversed. The measurement also

indicates that more $-V_g$ pulse counts are required to restore R_{xx} back to R_o (~36k pulses for $+V_g$ versus 10^6 pulses for $-V_g$). Notably, the asymmetric switching behavior is reminiscent with that obtained by IL gating. [13] While such an asymmetric switching is previously attributed to oxygen vacancies (V_o) created upon $+V_g$ applied in a vacuum environment ($<10^{-4}$ Torr), we argue that this is unlikely the sole mechanism in our case. The first reason is that, while a change of 45 % was recorded in Figure 3, this value is probably not the limit for ΔR_{xx}, judging from its linearly increasing trend. Besides, the asymmetric switching behavior can be observed as well under ambient gas conditions, which we will elucidate later. Most importantly, both the T_C and MR of the LSMO channel follow the reversibility of the voltage modulation closely (**Figure S3**).

One should, however, distinguish the above modulation strategy from that based on polarization switching in the ferroelectric polymer. According to our previous work, a saturating V_g in the order of ±35 V was necessary to reverse the ferroelectric dipoles in the copolymer at 300 K (Figure S1(b)). [34] Moreover, such a single pulse led to a change of R_{xx} by 15%, yet without any noticeable change in the T_C. Here, the small screening depth of electric field in conductive LSMO channel plays a role in these observations. For instance, based on the relation between the $\Delta\rho$ and ΔT_C discussed previously, the modulation induced by small voltage pulses enables $\Delta\rho$ as large as 7%, while it is less than 0.1 % for ferroelectric switching in P(VDF-TrFE) triggered by large gate voltages. [34]

3.3 Electrochemical Modulation of LSMO: A Simple Model

The magnetism of LSMO films depend heavily on the ratio of La^{2+} and Sr^{3+}, leading to the varying ratio of Mn^{3+} and Mn^{4+} valence states. [37] Apart from controlling the growth conditions of manganite films, [38, 39] electrostatic modulation of carrier concentration through ferroelectric

polarization has been previously reported. [20, 40, 41] Studies on the modulation by IL showed the possible generation of V_o by large V_g due to its small formation enthalpy. [13] However, this mechanism cannot fully account for the observations arising from low-V_g pulse chains, including asymmetric LSMO channel response between +/- V_g pulses cycles, reversible control of $\Delta R_{xx}/R_{xx}$ up to 45% and modulated ΔT_C by 15 K (Figure S1(b)).

The V_g–induced electrochemical reaction within the LSMO layer can be described as $Mn^{4+} \xrightarrow{+V_g} Mn^{4+}_{1-x} + Mn^{3+}_x + V_o^{2-} + O_2,$ [17, 42] suggesting the creation of oxygen vacancies V_o and thus Mn^{4+} to Mn^{3+} conversion. [35, 43] **Figure 4** visualizes these processes. Our model contains two LSMO interfaces, one in direct contact with P(VDF-TrFE), and the other with the STO substrate and thus unaffected by V_g. [44, 45] With +V_g pulses, n-type carriers in the form of V_o are created and gradually migrate to the inner film from the LSMO/P(VDF-TrFE) interface. The V_o diffusion could then alter the LSMO properties in two ways. First, because of the p-type nature of LSMO, the accumulated V_o induces additional resistance and drives the metallic channel into an insulating phase. V_o also leads to modulated T_C and MR ratio due to suppressed double exchange between Mn^{4+} and Mn^{3+}. Similar to electric field-control in LSMO through IL gating, [17] +V_g pulse chains induce decreased T_C, while higher T_C and lower MR ratio are expected for -V_g due to hole accumulation in the form of annihilated V_o, which enhances ferromagnetic coupling between Mn^{3+} and Mn^{4+} ions and suppresses magnetic scattering sites. [13]

Our model in Figure 4 is essentially electrochemical in nature rather than an electrostatic one. In practice, these have been distinguished from each other by comparing the V_g dependence of $\Delta R_{xx}/R_o$ in either oxygen-rich or vacuum environments (**Figure S4**). These results provide evidence of the electrochemical origin of our experimental observations, thus validating our

model in Figure 4. Our results also are in line with Ref. [13] that showed the electric field-induced reversible migration of V_o annihilation/formation in $La_{0.5}Sr_{0.5}CoO_{3-x}$ with IL gating.

3.4 Element-specific chemical and magnetic characterization of LSMO modulation

Figure 5(a) shows the Mn $2p$ XPS core-level spectra of pristine and $+V_g$-pulsed (36k) samples. Prior to the measurements, the copolymer gate dielectric and its top Al electrode were removed altogether in acetone after voltage pulsing. The Mn $2p_{3/2}$ peak of pristine sample is at 641.7 eV, but shifts towards a lower binding energy by 0.5±0.1 eV after gated with 36k $+V_g$ pulses. Quantitative peak fitting (Figure 5(b) and (c)) suggests a 41% decrease of the $Mn^{4+}/(Mn^{3+}+Mn^{4+})$ ratio [17] from 0.39±0.02 to 0.23±0.02, indicating a partial conversion of Mn^{4+} to Mn^{3+} upon the $+V_g$ pulses.

XA/XMCD measurements have been performed at 77 K to probe the magnetic responses of LSMO/P(VDF-TrFE) pulsed with V_g of opposite polarities, as shown in **Figure 6**(a) and 6(b). The spectral shapes (blue solid lines) are consistent with the previous work. [46] Closer inspection reveals a lower XMCD intensity for the $+V_g$-pulsed sample compared with the $-V_g$-pulsed one, which suggests a suppressed magnetic signal in the former. This is consistent with the observed lower T_C in the $+V_g$-pulsed sample as elaborated earlier. Using the XMCD sum rules analysis, [47-49] we estimate the ratio

$$\frac{m_L}{m_S+m_T} = \frac{1}{3-4.5(\frac{p}{q})},$$

(1)

where m_L and m_S are the orbital and spin moments, respectively. p is the integral of the dichroic signal of the L_3 peak alone and q is the integrated dichroism over both the L_3 and L_2 edges. [50] m_T corresponds to the magnetic spin dipole moment, arising from the anisotropy of the atomic charge distribution. [51] Here the incident X-ray angle of 60° is close to the magic angle (~55°),

11

where the contribution from m_T can be safely neglected, [47, 52] and accordingly the orbital-to-spin moment ratio $(\frac{m_L}{m_S})$ of Mn can be approximated using **Equation 1** as well.

As summarized in **Table 1**, $(\frac{m_L}{m_S})$ ratio of the pristine sample is very low, due to the effect of orbital quenching. [53] The application of $\pm V_g$ leads to an increase in the $(\frac{m_L}{m_S})$ ratio, which may arise from the evolution of V_o in LSMO (for $+V_g$ gating) or displaced oxygen atoms from the designated sites in the unit cells (for $-V_g$ gating).[54, 55] Density functional theory (DFT) calculation of LSMO/STO heterostructure [56] revealed that V_o results in an elongated octahedral along z direction, thus increasing m_L by suppressing the orbital quenching effect. [50] Meanwhile, we notice that the increasing degree of the $(\frac{m_L}{m_S})$ ratio in $+V_g$ sample is different from that in $-V_g$ sample. This could be related to the changes in the Mn^{3+}/Mn^{4+} ratio due to the presence of V_o. Through $+V_g$ pulsing, the increase in V_o lowers the concentration of Mn^{4+} in LSMO lattice, in turn resulting in the drop of m_S. [55] While through $-V_g$ pulsing, V_o are gradually eliminated albeit in a somewhat disordered manner compared with as-grown films, thus giving rise to an increase in m_S.

3.5 Discussion

The results in Figure S4, Figure 5 and Figure 6 provide strong support for the hypothesis of V_o formation and annihilation as the origin of modulated LSMO properties. Application of successive $+V_g$ pulses through the ferroelectric copolymer effectively drives oxygen out of the LSMO channel and creates V_o, accompanied by a valence transition of Mn^{4+} to Mn^{3+}. In contrast with Mn^{3+}-O-Mn^{4+} which favors ferromagnetic coupling, Mn^{3+}-O-Mn^{3+} leads to antiferromagnetic interaction. An increase in Mn^{3+}-O-Mn^{3+} coupling would result in the

suppressed magnetism of LSMO, as reflected from the reduced T_C and enhanced MR at 20 K. Transport and magnetic modulation in the LSMO channel through low-V_g pulsing across the P(VDF-TrFE) gate was presented in this work, and V_o generation/annihilation were observed. The LSMO channel behavior was due to electrochemical reactions, and this should be distinguished from that arising from the electrostatic effect due to ferroelectric polarization reversal in the copolymer dielectric. [41, 57] There are various reports on the use of ferroelectric gate dielectric for providing stable remanent polarization and achieving electrostatic switching of magnetism in transistor-type devices. [28, 40, 58] However, such devices are vulnerable to dielectric breakdown during the application of large saturation voltages. Such issues can be avoided by using the low-voltage pulse switching demonstrated in this work, which provides an alternative route for reliable, robust and efficient magnetism modulation in magnetic oxides.

The present study has focused on the demonstration of the pulsing effect with P(VDF-TrFE) as the gate dielectric. It would be of interest to understand if the technique can be extended to other gating materials; we have tried replacing P(VDF-TrFE) by poly(methyl methacrylate) (PMMA), and no modulation of T_C nor resistance in the LSMO channel was observed after 20k +V_g pulsing cycles. We speculate that materials with high dielectric constants would be more well-suited for the effect. Besides, oxygen or ionic porosity in the gate dielectric would allow the transport of oxygen across the gate dielectric/LSMO interface, facilitating the formation and annihilation of the oxygen vacancies in the channel layer.

4. CONCLUSION

To conclude, we fully characterized the reversible modulation of Tc and MR in LSMO thin films, through the application of moderate gate voltage pulse chains. XPS and XMCD results

suggested that the electric-field-induced modulation of magnetism were governed by creation and annihilation of V_o in LSMO channel, rather than electrostatic accumulation and depletion of charge carriers. This V_o modulation through low-voltage-pulsing method demonstrated the robust and reversible manipulation of transport and magnetism, providing a robust route to enhance the tunability of correlated oxide materials through control of V_o. This could be beneficial to develop novel electronic devices concepts.
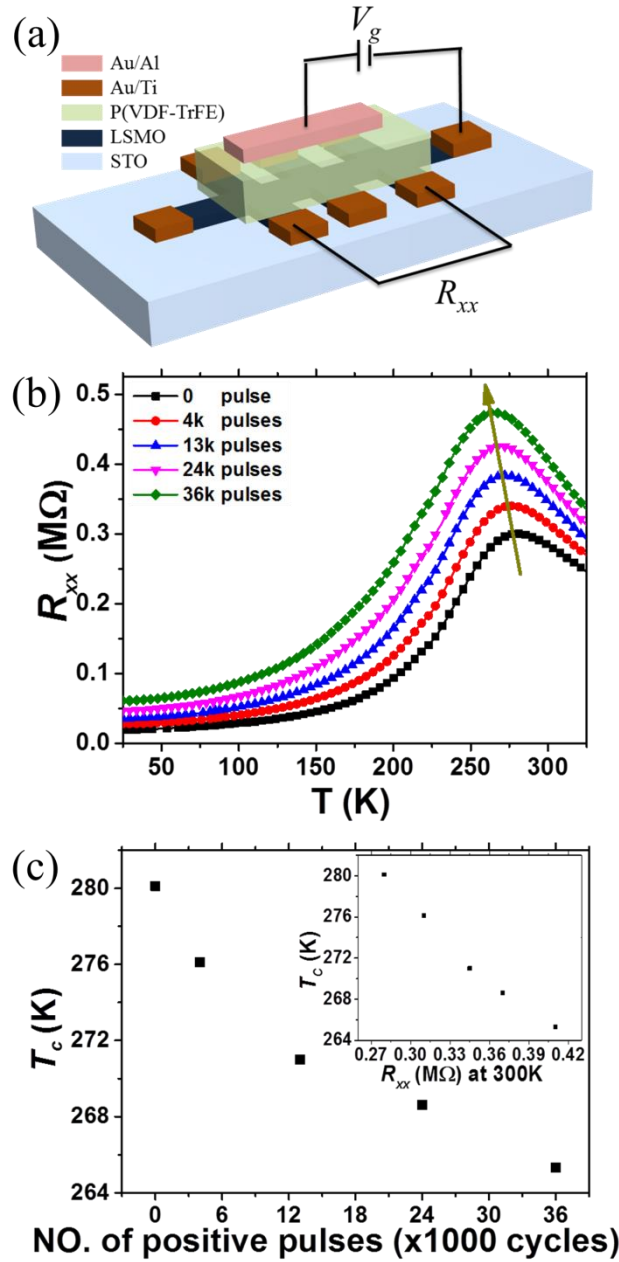
Figure 1. (a) Schematic diagram of LSMO field-effect device. (b) *R-T* measurement for sample undergone various $+V_g$ pulse chains. (c) *Tc* of LSMO channel as a function of $+V_g$ pulses (main figure) and R_{xx} at 300 K (inset).
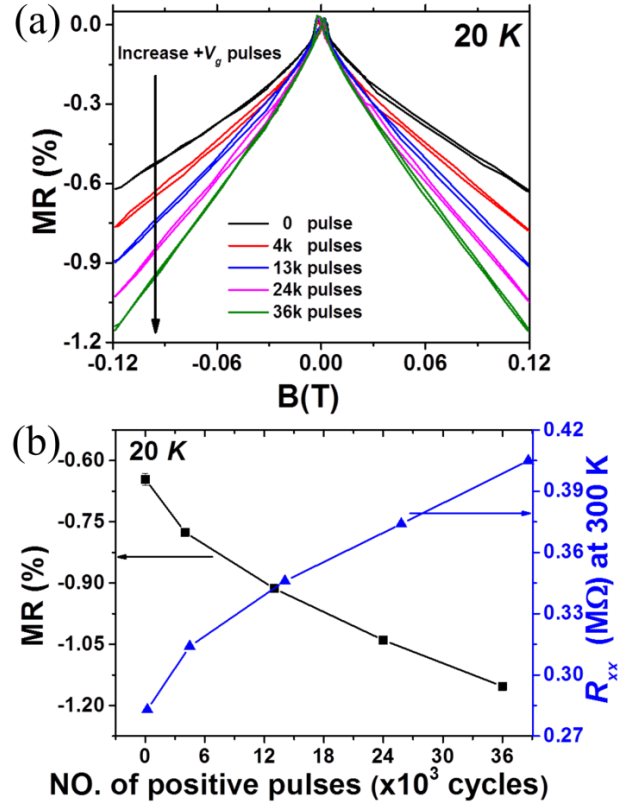
Figure 2. Variation of LSMO channel magnetotransport properties at 20 K with applied $+V_g$ pulses. (a) MR behavior for LSMO channel undergone $+V_g$ pulse chains; inset indicates the magnified view of MR loop after the application of 36k $+V_g$ pulses. (b) MR ratio (at 20 K) and R_{xx} (at 300 K) as a function of $+V_g$ pulse cycle.
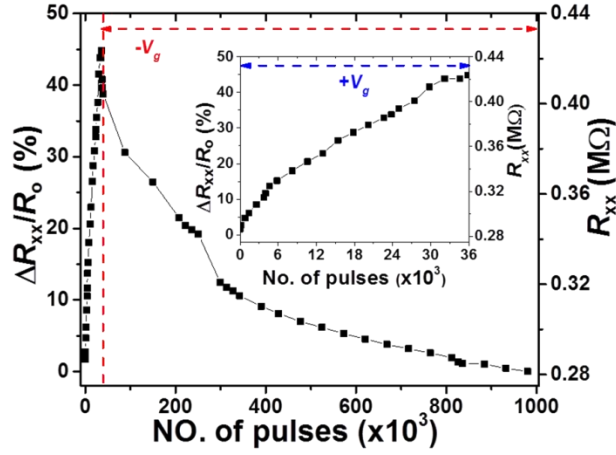
Figure 3. $\Delta R_{xx}/R_o$ (left axis) and R_{xx} at 300K (right axis) in response to successive $+V_g$ (first 36k) and $-V_g$ (up to 10^6) pulses with constant pulse widths (300 ms). Inset highlights $\Delta R_{xx}/R_o$ variation during the +10 V pulse cycles (at the beginning of the measurement in the main figure).
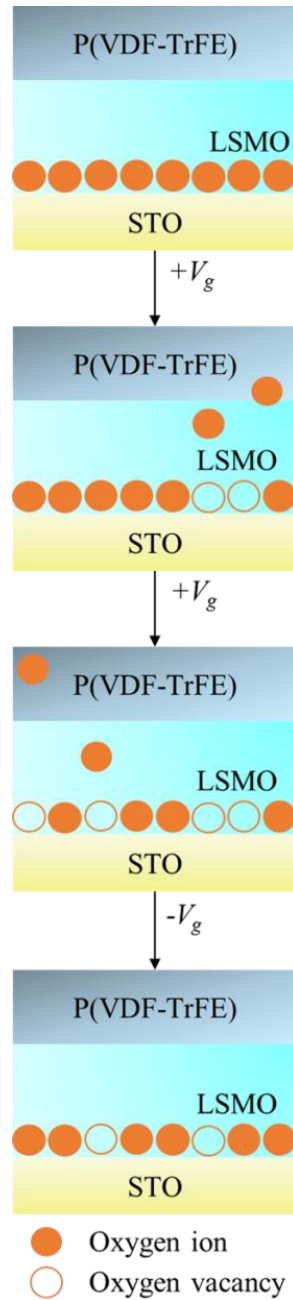
Figure 4. Evolution of V_o in LSMO channel with successive positive and negative V_g pulses, according to the proposed electrochemical switching mechanism.
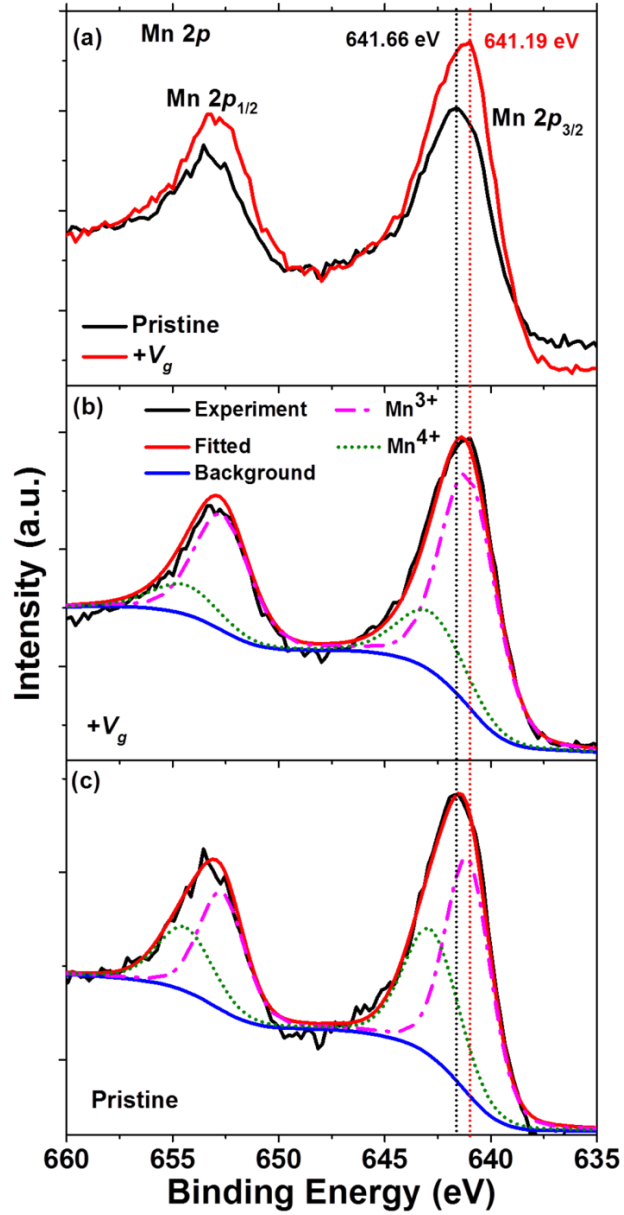
Figure 5. (a) Mn *2p* XPS spectra of LSMO film at pristine state and after $+V_g$ pulsing for 36k cycles. (b) and (c) show the multiple peak fitting of the XPS spectra for gated (b) and pristine (c) samples.
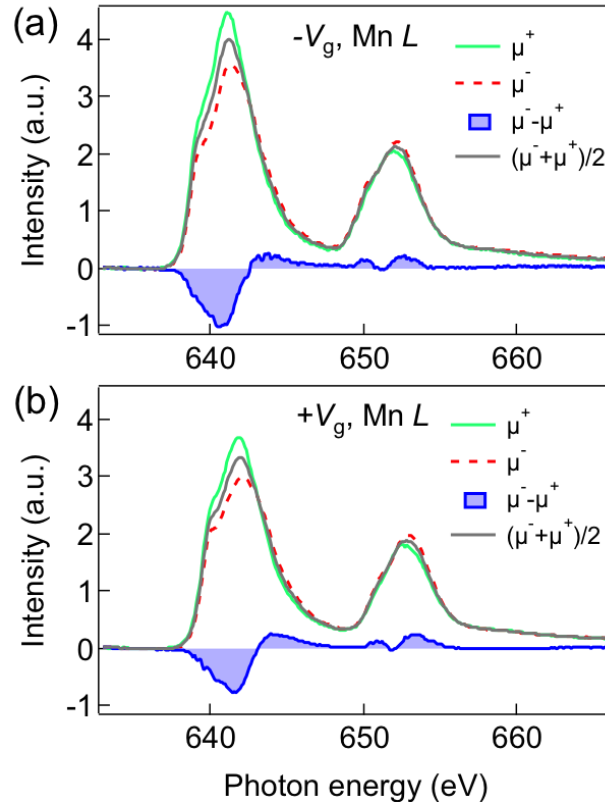
Figure 6. Mn $L_{2,3}$-edge XA/XMCD spectra of 7.5 nm LSMO undergone pulse switching by (a) -V_g and (b) +V_g, respectively, taken at 77 K. The XA spectra were taken with parallel (μ^-) and antiparallel (μ^+) alignment of the light helicity with respect to the applied magnetic field, and the XMCD was obtained by ($\mu^- - \mu^+$).

Table 1. $\frac{m_L}{m_S}$ ratio of pristine and +/- V_g-pulsed samples, as measured at the grazing incidence of

X-ray.

	Pristine	+V_g	-V_g
m_L/m_S	0.04	0.39	0.20

ASSOCIATED CONTENT

Supporting Information.

The Supporting Information is available free of charge.

Structural and ferroelectric characterization of LSMO films on STO and P(VDF-TrFE) on LSMO device; characterization of field-effect devices with V_g pulses; reversible modulation of LSMO channel properties; modulation of R_{xx} under oxygen and vacuum ambient conditions.

AUTHOR INFORMATION

Corresponding Author

Chi Wah Leung - Department of Applied Physics, The Hong Kong Polytechnic University, Hung Hom, Kowloon, Hong Kong, China

Email: dennis.leung@polyu.edu.hk

Author Contributions

Hon Fai Wong - *Department of Applied Physics, The Hong Kong Polytechnic University, Hung Hom, Kowloon, Hong Kong, China*

Sheung Mei Ng - *Department of Applied Physics, The Hong Kong Polytechnic University, Hung Hom, Kowloon, Hong Kong, China*

Wen Zhang - *School of Electronics and Information and School of Microelectronics, Northwestern Polytechnical University, 127 West Youyi Road, Xi'an, Shaanxi, 710072, China; Department of Physics, National University of Singapore, 2 Science Drive 3, Singapore 117542, Singapore*

Yu Kuai Liu - *Department of Applied Physics, The Hong Kong Polytechnic University, Hung Hom, Kowloon, Hong Kong, China*

Ping Kwan Johnny Wong - *School of Electronics and Information and School of Microelectronics, Northwestern Polytechnical University, 127 West Youyi Road, Xi'an, Shaanxi, 710072, China; Centre for Advanced 2D Materials and Graphene Research Centre, National University of Singapore, 6 Science Drive 2, Singapore 117546, Singapore*

Chi Sin Tang - *Department of Physics, National University of Singapore, 2 Science Drive 3, Singapore 117542, Singapore*

Ka Kin Lam - *Department of Applied Physics, The Hong Kong Polytechnic University, Hung Hom, Kowloon, Hong Kong, China*

Xu Wen Zhao - *Department of Applied Physics, The Hong Kong Polytechnic University, Hung Hom, Kowloon, Hong Kong, China*

Zhen Gong Meng - *College of Chemistry and Environmental Engineering, Shenzhen University, Shenzhen 518060, China*

Lin Feng Fei - *Department of Applied Physics, The Hong Kong Polytechnic University, Hung Hom, Kowloon, Hong Kong, China*

Wang Fai Cheng - *Department of Applied Physics, The Hong Kong Polytechnic University, Hung Hom, Kowloon, Hong Kong, China*

Danny von Nordheim - *Department of SciTec, University of Applied Sciences Jena, Carl-Zeiss-Promenade 2, 07743 Jena, Germany*

Wai Yeung Wong- *Department of Applied Biology and Chemical Technology, The Hong Kong Polytechnic University, Hung Hom, Hong Kong, China*

Zong Rong Wang- *State Key Lab of Silicon Materials, School of Materials Science and Engineering, Zhejiang University, Hangzhou, China*

Bernd Ploss - *Department of SciTec, University of Applied Sciences Jena, Carl-Zeiss-Promenade 2, 07743 Jena, Germany*

Ji-Yan Dai - *Department of Applied Physics, The Hong Kong Polytechnic University, Hung Hom, Kowloon, Hong Kong, China*

Chee Leung Mak - *Department of Applied Physics, The Hong Kong Polytechnic University, Hung Hom, Kowloon, Hong Kong, China*

Andrew Thye Shen Wee - *Department of Physics, National University of Singapore, 2 Science Drive 3, Singapore 117542, Singapore; Centre for Advanced 2D Materials and Graphene Research Centre, National University of Singapore, 6 Science Drive 2, Singapore 117546, Singapore*

Author Contributions

H.F. Wong and S.M. Ng carried out sample fabrication and transport measurement. W. Zhang, P.K.J. Wong, C.S. Tang and A.T.S. Wee performed the XMCD measurement. Y.K. Liu, K.K. Lam, X.W. Zhao, W.F. Cheng and C.L. Mak carried out AFM and XRD works. D.V. Nordheim, Z.R. Wang and B. Ploss conducted copolymer preparation and the piezoelectric measurement. J.Y. Dai performed the TEM measurement. H.F. Wong and C.W. Leung designed and organized the study and wrote the manuscript. All authors involved in discussion of the results and gave advice on the manuscript.

Notes

The authors declare no competing financial interest.

REFERENCES

(1)   Hemberger, J.; Krimmel, A.; Kurz, T.; Krug von Nidda, H. A.; Ivanov, V. Y.; Mukhin, A. A.; Balbashov, A. M.; Loidl, A. Structural, magnetic, and electrical properties of single-crystalline $La_{1-x}Sr_xMnO_3$ (0.4<x<0.85). *Phys. Rev. B* **2002**, 66, 094410.

(2)   Wang, X. L.; Lai, K. H.; Ruotolo, A. A comparative study on the ferromagnetic properties of undoped and Mn-doped ZnO. *J. Alloy. Compd*. **2012**, 542, 147-150.

(3)   Wang, X. L.; Shao, Q.; Zhuravlyova, A.; He, M.; Yi, Y.; Lortz, R.; Wang, J. N.; Ruotolo, A. Giant negative magnetoresistance in Manganese-substituted Zinc Oxide. *Sci. Rep*. **2015**, 5, 9221.

(4)   Urushibara, A.; Moritomo, Y.; Arima, T.; Asamitsu, A.; Kido, G.; Tokura, Y. Insulator-metal transition and giant magnetoresistance in $La_{1-x}Sr_xMnO_3$. *Phys. Rev. B* **1995**, 51, 14103-14109.

(5)   Ahn, C. H.; Bhattacharya, A.; Di Ventra, M.; Eckstein, J. N.; Frisbie, C. D.; Gershenson, M. E.; Goldman, A. M.; Inoue, I. H.; Mannhart, J.; Millis, A. J.; Morpurgo, A. F.; Natelson, D.; Triscone, J.-M. Electrostatic modification of novel materials. *Rev. Mod. Phys*. **2006**, 78, 1185-1212.

(6)   Ahn, C. H.; Triscone, J. M.; Mannhart, J. Electric field effect in correlated oxide systems. *Nature* **2003**, 424, 1015-1018.

(7)   Hong, X.; Posadas, A.; Lin, A.; Ahn, C. H. Ferroelectric-field-induced tuning of magnetism in the colossal magnetoresistive oxide $La_{1-x}Sr_xMnO_3$. *Phys. Rev. B* **2003**, 68, 134415.

(8)   Galiński, M.; Lewandowski, A.; Stępniak, I. Ionic liquids as electrolytes. *Electrochim. Acta* **2006**, 51, 5567-5580.

(9)   Fujimoto, T.; Awaga, K. Electric-double-layer field-effect transistors with ionic liquids. *Phys. Chem. Chem. Phys*. **2013**, 15, 8983-9006.

(10)   Jeong, J.; Aetukuri, N.; Graf, T.; Schladt, T. D.; Samant, M. G.; Parkin, S. S. P. Suppression of Metal-Insulator Transition in VO_2 by Electric Field–Induced Oxygen Vacancy Formation. *Science* **2013**, 339, 1402-1405.

(11)   Schladt, T. D.; Graf, T.; Aetukuri, N. B.; Li, M.; Fantini, A.; Jiang, X.; Samant, M. G.; Parkin, S. S. P. Crystal-Facet-Dependent Metallization in Electrolyte-Gated Rutile TiO_2 Single Crystals. *ACS Nano* **2013**, 7, 8074-8081.

(12)   Zhou, Y.; Park, J.; Shi, J.; Chhowalla, M.; Park, H.; Weitz, D. A.; Ramanathan, S. Control of Emergent Properties at a Correlated Oxide Interface with Graphene. *Nano Lett*. **2015**, 15, 1627-1634.

(13)   Walter, J.; Wang, H.; Luo, B.; Frisbie, C. D.; Leighton, C. Electrostatic versus Electrochemical Doping and Control of Ferromagnetism in Ion-Gel-Gated Ultrathin $La_{0.5}Sr_{0.5}CoO_{3−δ}$. *ACS Nano* **2016**, 10, 7799-7810.

(14)   Passarello, D.; Altendorf, S. G.; Jeong, J.; Samant, M. G.; Parkin, S. S. P. Metallization of Epitaxial VO_2 Films by Ionic Liquid Gating through Initially Insulating TiO2 Layers. *Nano Lett*. **2016**, 16, 5475-5481.

(15)   Ji, H.; Wei, J.; Natelson, D. Modulation of the Electrical Properties of VO_2 Nanobeams Using an Ionic Liquid as a Gating Medium. *Nano Lett*. **2012**, 12, 2988-2992.

(16)   Wang, Y.; Zhou, X.; Song, C.; Yan, Y.; Zhou, S.; Wang, G.; Chen, C.; Zeng, F.; Pan, F. Electrical Control of the Exchange Spring in Antiferromagnetic Metals. *Adv. Mater*. **2015**, 27, 3196-3201.

(17)   Cui, B.; Song, C.; Wang, G.; Yan, Y.; Peng, J.; Miao, J.; Mao, H.; Li, F.; Chen, C.; Zeng, F.; Pan, F. Reversible Ferromagnetic Phase Transition in Electrode-Gated Manganites. *Adv. Funct. Mater*. **2014**, 24, 7233-7240.

(18)   Ye, J. T.; Inoue, S.; Kobayashi, K.; Kasahara, Y.; Yuan, H. T.; Shimotani, H.; Iwasa, Y. Liquid-gated interface superconductivity on an atomically flat film. *Nat. Mater*. **2010**, 9, 125-128.

(19)   Shiogai, J.; Ito, Y.; Mitsuhashi, T.; Nojima, T.; Tsukazaki, A. Electric-field-induced superconductivity in electrochemically etched ultrathin FeSe films on $SrTiO_3$ and MgO. *Nat. Phys*. **2016**, 12, 42-46.

(20)   Lu, H.; George, T. A.; Wang, Y.; Ketsman, I.; Burton, J. D.; Bark, C.-W.; Ryu, S.; Kim, D. J.; Wang, J.; Binek, C.; Dowben, P. A.; Sokolov, A.; Eom, C.-B.; Tsymbal, E. Y.; Gruverman, A. Electric modulation of magnetization at the $BaTiO_3$/$La_{0.67}Sr_{0.33}MnO_3$ interfaces. *Appl. Phys. Lett.* **2012**, 100, 232904.

(21)   Wu, S. M.; Cybart, S. A.; Yi, D.; Parker, J. M.; Ramesh, R.; Dynes, R. C. Full Electric Control of Exchange Bias. *Phys. Rev. Lett*. **2013**, 110, 067202.

(22)   Wu, T.; Ogale, S. B.; Garrison, J. E.; Nagaraj, B.; Biswas, A.; Chen, Z.; Greene, R. L.; Ramesh, R.; Venkatesan, T.; Millis, A. J. Electroresistance and Electronic Phase Separation in Mixed-Valent Manganites. *Phys. Rev. Lett*. **2001**, 86, 5998-6001.

(23)   Cui, B.; Song, C.; Mao, H.; Wu, H.; Li, F.; Peng, J.; Wang, G.; Zeng, F.; Pan, F. Magnetoelectric Coupling Induced by Interfacial Orbital Reconstruction. *Adv. Mater*. **2015**, 27, 6651-6656.

(24)   Persano, L.; Dagdeviren, C.; Su, Y.; Zhang, Y.; Girardo, S.; Pisignano, D.; Huang, Y.; Rogers, J. A. High performance piezoelectric devices based on aligned arrays of nanofibers of poly(vinylidenefluoride-co-trifluoroethylene). *Nat. Commun*. **2013**, 4, 1633.

(25)   Ploss, B.; Ploss, B. Dielectric nonlinearity of PVDF–TrFE copolymer. *Polymer* **2000**, 41, 6087-6093.

(26)   Von Nordheim, D.; Hahne, S.; Ploss, B. Polarisation Readout and Determination of Landau Parameters of VDF-TrFE Thin Films from Dielectric Nonlinearities. *Ferroelectrics* **2013**, 453, 122-126.

(27)   Hu, W. J.; Juo, D.-M.; You, L.; Wang, J.; Chen, Y.-C.; Chu, Y.-H.; Wu, T. Universal Ferroelectric Switching Dynamics of Vinylidene Fluoride-trifluoroethylene Copolymer Films. *Sci. Rep*. **2014**, 4, 4772.

(28)   Stolichnov, I.; Riester, S. W. E.; Trodahl, H. J.; Setter, N.; Rushforth, A. W.; Edmonds, K. W.; Campion, R. P.; Foxon, C. T.; Gallagher, B. L.; Jungwirth, T. Non-volatile ferroelectric control of ferromagnetism in (Ga,Mn)As. *Nat. Mater.* **2008**, 7, 464-467.

(29)   Lau, H. K.; Leung, C. W. Nonvolatile multilevel memory effect by resistive switching in manganite thin films. *J. Appl. Phys*. **2008**, 104, 123705.

(30)   Ruotolo, A.; Leung, C. W.; Lam, C. Y.; Cheng, W. F.; Wong, K. H.; Pepe, G. P. Unification of bulk and interface electroresistive switching in oxide systems. *Phys. Rev. B* **2008**, 77, 233103.

(31)   Cheng, W. F.; Ruotolo, A.; Chan, Y. K.; Wong, K. H.; Leung, C. W. Spacerless metal-manganite pseudo-spin-valve structure. *J. Appl. Phys.* **2008**, 103, 103903.

(32)   Liao, Z.; Zhang, J., Metal-to-Insulator Transition in Ultrathin Manganite Heterostructures. *Appl. Sci.* **2019**, 9, 144.

(33).   Yu, X.; Wilhelmi, O.; Moser, H. O.; Vidyaraj, S. V.; Gao, X.; Wee, A. T. S.; Nyunt, T.; Qian, H.; Zheng, H. New soft X-ray facility SINS for surface and nanoscale science at SSLS. *J. Electron Spectrosc.* **2005**, 144-147, 1031-1034.

(34)   Wong, H. F.; Ng, S. M.; Cheng, W. F.; Liu, Y.; Chen, X.; von Nordheim, D.; Mak, C. L.; Dai, J.; Ploss, B.; Leung, C. W. Enhanced tunability of electrical and magnetic properties in (La,Sr)MnO$_3$ thin films via field-assisted oxygen vacancy modulation. *Solid-State Electron.* **2017**, 138, 56-61.

(35)   Huang, M.; Tan, A. J.; Mann, M.; Bauer, U.; Ouedraogo, R.; Beach, G. S. D. Three-terminal resistive switch based on metal/metal oxide redox reactions. *Sci. Rep.* **2017**, 7, 7452.

(36)   Zhou, Y.; Zhu, X.; Li, S. Effect of heat treatment condition on magnetic, electrical transport and magnetoresistance properties of La0.67Sr0.33MnO3 manganite coatings. *Ceram. Int.* **2018**, 44, 15010-15018.

(37)   Zener, C. Interaction between the d-Shells in the Transition Metals. II. Ferromagnetic Compounds of Manganese with Perovskite Structure. *Phys. Rev.* **1951**, 82, 403-405.

(38)   Cheng, W.F.; Leung, C.W. Effect of post annealing on La0.7Sr0.3MnO3 thin films. *Acta Phys. Pol. A* **2007**, 111, 117.

(39)   Dho, J.; Hur, N. H.; Kim, I. S.; Park, Y. K. Oxygen pressure and thickness dependent lattice strain in La0.7Sr0.3MnO3 films. *J. Appl. Phys.* **2003**, 94, 7670-7674.

(40)   Kanki, T.; Tanaka, H.; Kawai, T. Electric control of room temperature ferromagnetism in a Pb(Zr$_{0.2}$Ti$_{0.8}$)O$_3$/La$_{0.85}$Ba$_{0.15}$MnO$_3$ field-effect transistor. *Appl. Phys. Lett.* **2006**, 89, 242506.

(41)   Kanki, T.; Park, Y.-G.; Tanaka, H.; Kawai, T. Electrical-field control of metal–insulator transition at room temperature in Pb(Zr$_{0.2}$Ti$_{0.8}$)O$_3$/La$_{1−x}$Ba$_x$MnO$_3$ field-effect transistor. *Appl. Phys. Lett.* **2003**, 83, 4860-4862.

(42)   Ge, C.; Jin, K.-J.; Gu, L.; Peng, L.-C.; Hu, Y.-S.; Guo, H.-Z.; Shi, H.-F.; Li, J.-K.; Wang, J.-O.; Guo, X.-X.; Wang, C.; He, M.; Lu, H.-B.; Yang, G.-Z. Metal–Insulator Transition Induced

by Oxygen Vacancies from Electrochemical Reaction in Ionic Liquid-Gated Manganite Films. *Adv. Mater. Interfaces* **2015**, 2, 1500407.

(43)   Nian, Y. B.; Strozier, J.; Wu, N. J.; Chen, X.; Ignatiev, A. Evidence for an Oxygen Diffusion Model for the Electric Pulse Induced Resistance Change Effect in Transition-Metal Oxides. *Phys. Rev. Lett.* **2007**, 98, 146403.

(44)   Nakano, M.; Shibuya, K.; Okuyama, D.; Hatano, T.; Ono, S.; Kawasaki, M.; Iwasa, Y.; Tokura, Y. Collective bulk carrier delocalization driven by electrostatic surface charge accumulation. *Nature* **2012**, 487, 459.

(45)   Dhoot, A. S.; Israel, C.; Moya, X.; Mathur, N. D.; Friend, R. H. Large Electric Field Effect in Electrolyte-Gated Manganites. *Phys. Rev. Lett*. **2009**, 102, 136402.

(46)   de Jong, M. P.; Bergenti, I.; Dediu, V. A.; Fahlman, M.; Marsi, M.; Taliani, C. Evidence for Mn^{2+} ions at surfaces of $La_{0.7}S_{0.3}MnO_3$ thin films. *Phys. Rev. B* **2005**, 71, 014434.

(47)   Stöhr, J.; König, H. Determination of Spin- and Orbital-Moment Anisotropies in Transition Metals by Angle-Dependent X-Ray Magnetic Circular Dichroism. *Phys. Rev. Lett.* **1995**, 75, 3748-3751.

(48)   Thole, B. T.; Carra, P.; Sette, F.; van der Laan, G. X-ray circular dichroism as a probe of orbital magnetization. *Phys. Rev. Lett.* **1992**, 68, 1943-1946.

(49)   Stöhr, J. X-ray magnetic circular dichroism spectroscopy of transition metal thin films. *J. Electron Spectrosc.* **1995**, 75, 253-272.

(50)   Aruta, C.; Ghiringhelli, G.; Bisogni, V.; Braicovich, L.; Brookes, N. B.; Tebano, A.; Balestrino, G. Orbital occupation, atomic moments, and magnetic ordering at interfaces of manganite thin films. *Phys. Rev. B* **2009**, 80, 014431.

(51)   Zhang, W.; Wong, P. K. J.; Zhou, X.; Rath, A.; Huang, Z.; Wang, H.; Morton, S. A.; Yuan, J.; Zhang, L.; Chua, R.; Zeng, S.; Liu, E.; Xu, F.; Ariando; Chua, D. H. C.; Feng, Y. P.; van der Laan, G.; Pennycook, S. J.; Zhai, Y.; Wee, A. T. S. Ferromagnet/Two-Dimensional Semiconducting Transition-Metal Dichalcogenide Interface with Perpendicular Magnetic Anisotropy. *ACS Nano* **2019**, 13, 2253-2261.

(52)   Dürr, H. A.; van der Laan, G. Magnetic circular x-ray dichroism in transverse geometry: Importance of noncollinear ground state moments. *Phys. Rev. B* **1996**, 54, R760-R763.

(53)   Preziosi, D.; Alexe, M.; Hesse, D.; Salluzzo, M. Electric-Field Control of the Orbital Occupancy and Magnetic Moment of a Transition-Metal Oxide. *Phys. Rev. Lett*. **2015**, 115, 157401.

(54)   Guo, H.; Wang, J.-o.; He, X.; Yang, Z.; Zhang, Q.; Jin, K.-j.; Ge, C.; Zhao, R.; Gu, L.; Feng, Y.; Zhou, W.; Li, X.; Wan, Q.; He, M.; Hong, C.; Guo, Z.; Wang, C.; Lu, H.; Ibrahim, K.; Meng, S.; Yang, H.; Yang, G. The Origin of Oxygen Vacancies Controlling La2/3Sr1/3MnO3 Electronic and Magnetic Properties. *Adv. Mater. Interfaces* **2016**, 3, 1500753.

(55)   Koide, T.; Miyauchi, H.; Okamoto, J.; Shidara, T.; Sekine, T.; Saitoh, T.; Fujimori, A.; Fukutani, H.; Takano, M.; Takeda, Y. Close Correlation between the Magnetic Moments, Lattice Distortions, and Hybridization in $LaMnO_3$ and $La_{1-x}Sr_xMnO_{3+\delta}$: Doping-Dependent Magnetic Circular X-Ray Dichroism Study. *Phys. Rev. Lett.* **2001**, 87, 246404.

(56)   Nord, M.; Vullum, P. E.; Moreau, M.; Boschker, J. E.; Selbach, S. M.; Holmestad, R.; Tybell, T. Structural phases driven by oxygen vacancies at the $La_{0.7}Sr_{0.3}MnO_3$/$SrTiO_3$ hetero-interface. *Appl. Phys. Lett.* **2015**, 106, 041604.

(57)   Chiba, D.; Matsukura, F.; Ohno, H. Electric-field control of ferromagnetism in (Ga,Mn)As. *Appl. Phys. Lett.* **2006**, 89, 162505.

(58) Zhao, T.; Ogale, S. B.; Shinde, S. R.; Ramesh, R.; Droopad, R.; Yu, J.; Eisenbeiser, K.;

Misewich, J. Colossal magnetoresistive manganite-based ferroelectric field-effect transistor on Si.

Appl. Phys. Lett. **2004**, 84, 750-752.